Journal of Applied Polymer Science

Electrical conductivity and mechanical performance of multiwalled CNT-filled polyvinyl chloride composites subjected to tensile load

Hessam Yazdani,[1,3] Benjamin E Smith,[2] Kianoosh Hatami[3]

[1]Department of Civil and Environmental Engineering, Howard University, 2300 Sixth Street NW, Washington, DC 20059
[2]Samuel Roberts Noble Microscopy Laboratory, the University of Oklahoma, 770 Van Vleet Oval, Norman, Oklahoma 73019
[3]School of Civil Engineering and Environmental Science, the University of Oklahoma, 202 W Boyd St, Room 450B, Norman, Oklahoma 73019
Correspondence to: K. Hatami (E-mail: kianoosh@ou.edu)

ABSTRACT: This article reports a study on the strain-sensitive conductivity (tensoresistivity) and mechanical properties of polyvinyl chloride/multiwalled carbon nanotube (PVC/MWCNT) composites subjected to tensile loading at different strain rates for potential use in sensor-enabled geosynthetics and other applications involving electrically conductive polymer composites. Results indicate that adding 0.5 wt % MWCNT to the composite results in 57% reduction in its ultimate (failure) strain and a fivefold increase in its tensile modulus while leaving its ultimate strength almost unchanged. Laser scanning confocal microscopy is used to investigate the microscopic failure mechanism of the composite and how it contributes to the strain-sensitive conductivity of the composites. It is observed that tensile fractures are initiated from inside the largest bundles between 18% and 36% strain and continue through further fractal-like fracturing in smaller bundles. Gauge factors (e.g., 3.17) comparable to or exceeding those of typical strain gauges are obtained for the composite, indicating its strong potential for structural performance monitoring and damage detection applications.
 J. Appl. Polym. Sci. **2016**, *133*, 43665.

KEYWORDS: composites; conducting polymers; graphene and fullerenes; mechanical properties; microscopy; nanotubes

Received 4 December 2015; accepted 22 March 2016
DOI: 10.1002/app.43665

INTRODUCTION

Conductive polymer composites (CPCs) are conductor-insulator heterogeneous materials that result from dispersing conductive nanofillers such as carbon blacks (CBs) and carbon nanotubes (CNTs) within an insulating polymer [e.g., polyvinyl chloride (PVC)]. In CPCs, a sufficient quantity of a nanofiller forms a continuous conducting network which provides relatively low-resistance electrical paths for free movement of electrons or very small interaggregate gaps across which electrons can hop by tunneling. The minimum concentration of conductive particles corresponding to the formation of a continuous interconnecting network of particles is known as the percolation threshold, where a sudden and substantial rise in the electrical conductivity of the composite is observed. Doping CPCs at a critical filler concentration slightly greater than the percolation threshold could impart tensoresistivity (strain-sensitive conductivity) to CPCs. By tensoresistivity, we refer to a proportional increase in the electrical resistance of a material when stretched as opposed to piezoresistivity which demonstrates the pressure-induced reduction in electrical resistance.[1]

Strain-sensitive conductivity paired with other desirable characteristics (e.g., flexibility, affordability, durability, and compatibility with structural materials) make CPCs technologically and economically attractive materials in a variety of applications such as thermal interfacing and electromagnetic shielding.[2] Particularly, the development of CPCs filled with carbonaceous fillers has given rise to the emergence of multifunctional smart materials as an alternative to the conventional strain-sensing instruments (e.g., strain gauges[3,4]). In addition, the emerging technology of fabrics with integrated sensors has paved the way for a number of potential applications such as smart shirts designed to monitor the physiological statistics of patients or

Additional Supporting Information may be found in the online version of this article.

fabric-based sensor nets capable of detecting cloaked enemies.[5–7] The strain-sensing capability of CPCs could be exceptional, with gauge factors as large as 700 (as opposed to a typical value of 2 for commercial strain gauges) for cement-based materials.[8] By definition, gauge factor is the relative change in a specimen's electrical resistance per unit strain as[9]:

$$\mathrm{GF} = \frac{\Delta R/R_0}{\varepsilon} \quad (1)$$

where ΔR is the difference between the current resistance and initial/unstrained resistance (R_0) and ε is strain.

Geosynthetics are polymeric products that are extensively used in geotechnical, transportation, and environmental engineering applications ranging from stabilizing highway embankments, bridge abutments and roadway subgrades to landfills, dams and irrigation canals, and fish farms. Currently, strain gauges and extensometers are commonly used to measure strains in geosynthetics by attaching them to geosynthetic layers at desired locations.[10,11] However, widespread use of these instruments in civil engineering projects has been hindered by several shortcomings including: (1) they usually require complex and expensive data acquisition systems, (2) their in-isolation (in-air) calibration factors could be inaccurate for in-soil applications as a result of local stiffening and in-soil interactions of their protective assemblies, and (3) strain gauges typically pose durability and survivability challenges for long-term monitoring of deformations especially at larger strains.[12]

To address the above challenges to widespread performance monitoring of geotechnical projects involving geosynthetics, the authors and colleagues have developed a new technology, termed as sensor-enabled geosynthetics (SEG), in the past few years. SEG materials include an optimal concentration of electrically conductive fillers (e.g., CB or CNT) which affords them a strain-sensing capability in addition to their conventional geosynthetic functions. This capability allows geosynthetic strains to be measured more conveniently and economically as compared to the use of conventional instruments. It is worth noting that CB has traditionally been used in conventional geosynthetics as a UV-absorbent to protect the products from damaging UV radiation. Therefore, using CB is SEG would require little modification in the existing production processes for geosynthetics. Also, since the cost of CB is only a minute fraction of the total cost of the products, a small adjustment in its concentration is not expected to add any significant amount to the total cost of geosynthetics production.

The SEG technology was first proposed by Hatami *et al.*[12,13] who carried out a proof-of-concept study to examine the potential of CPCs to add a self-sensing function to conventional geosynthetics. Hatami *et al.*[12,13] investigated the tensoresistive properties of CB- and CNT-filled high-density polyethylene (HDPE) and polypropylene (PP) composites. Their results showed that, except for CNT-filled PP composites, all other composites, especially the CB-filled specimens, exhibit tensoresistivities adequate for strain-sensing applications.

A major application of SEG is in geogrids, which are used for soil reinforcement in highway slopes, pavements and landfills among other applications. Geogrids are commonly made of PP, polyethylene (PE) or PVC-coated polyester. Unitized geogrids are made by heat-welding PP or PE strips (bonded geogrids) or stretching a needle-punched PP or PE sheet into a grid (extruded geogrids). Fathi *et al.*[14] and Yazdani *et al.*[15] studied the percolation threshold, mechanical properties, and tensoresistivity of CB-filled low-density PE and PP composites for potential use in unitized sensor-enabled geogrids (SEGG).

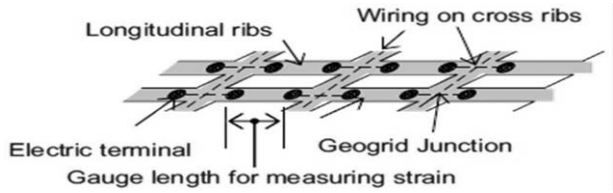

Figure 1. Schematic diagram of SEG ribs which do not require external sensors and protective assembly to measure strains in the geogrid ribs.[12]

In contrast to unitized geogrids, woven, and knitted geogrids are produced by interlacing high-tenacity PET yarns into an open structure and coating them with a CB-filled PVC composite. This coating protects polyester yarns against deleterious effects of water and chemically aggressive environments, UV rays and those from impact loads during installation and construction. Other additives are also used in the formulation of the PVC coating to improve its pliability and fire resistance, among others.[16] Hatami *et al.*[1] added an optimal concentration of CB to PVC to produce UV-protected and tensoresistive woven and knitted SEGG. The tensoresistive response of woven and knitted SEGG to cyclic loading and confining pressure was later studied by Yazdani *et al.*[9,17]

Major advantages of SEGG over existing instrumentation practice (primarily, use of strain gauges on geogrids) can be summarized as follows:

a. Conventional sensors such as strain gauges require fairly complex and expensive data acquisition (DAQ) systems. They also need an excitation voltage to operate. In contrast, only an ohmmeter would be needed to measure the electrical resistance between any two points defining a desired gauge length on the SEGG material (e.g., geogrid ribs shown in Figure 1)
b. strain gauges calibrated in air have to be protected against damage using plastic tubing filled with silicone gel or similar provisions (Figure 2). As a result, the entire process of using an adhesive to attach an external element such as a strain gauge to the measurement point on the geogrid and subsequent attachment of a bulky protection assembly results in a significantly different rigidity and interlocking properties with the adjacent soil and aggregates in actual field application as compared to an otherwise intact rib in a comparable location on the geogrid layer. Consequently, the in-air calibration factors are likely to be quite different from the values that need to be applied when the geogrid strain is measured in an embedded condition under confining pressure.

In contrast, the SEGG ribs will be left untouched and exposed when embedded in soil. There will not be any

adhesives, attached sensors (e.g., strain gauges) or bulky assemblies to protect the external sensors on the geogrid ribs. Therefore, the measurement point at the middle of an embedded SEGG geogrid rib will perform very similar to its in-air condition, thereby eliminating the corresponding sources of error in the measured strain data.

c. Strain gauges used on geogrids are typically reliable for a limited range of strains (3–5%), as they become detached or suffer other modes of failure at higher strains. In contrast, the authors' extensive data on a wide range of SEG prototypes to date have shown reliable tensoresistivity up to 10% strains or higher.[1,9,12,14,17]

To the best of the authors' knowledge, although electrical properties of CNT-filled PVC composites have been the subject of a few studies,[18–20] their mechanical properties and strain sensitivity have not been investigated. Hence, a primary objective of this study was to examine the mechanical properties and strain-sensitive electrical conductivity of CNT-filled PVC coating composites through a series of tensile tests at different strain rates while their conductivity was measured simultaneously. The materials and fabrication techniques specifically used in this study are based on the results obtained and described by the authors,[21] where different processing and dispersion methods were examined to obtain MWCNT/PVC composites that would exhibit the most desirable and repeatable electrical and mechanical properties. Additionally, the microscopy technique recently developed by the authors[22] was used to measure the conductivity response of an MWCNT/PVC composite sample with the most desirable properties subjected to tensile load in real time and under a laser scanning confocal microscope. The microscopy technique was used to better understand: (1) how microstructural changes contribute to the strain-dependent conductivity of the filled composites and, (2) the influences of the size and distribution of CNT bundles on the failure mechanism of the CNT-filled composites.

EXPERIMENTAL

Materials

PVC plastisol in liquid form (denoted here as PL) with a density $\rho_p = 1.37$ g/cc was used as the polymer matrix of the coating composite. PL consists of PVC resin suspended in a compatible plasticizer. Multiwalled carbon nanotubes (MWCNTs) with the properties as given in Table I were used as the filler. The density of the MWCNT was assumed to be the same as, or at least comparable to that of pure graphite (i.e., $\rho_f = 2.045$ g/cc[19]). An auxiliary plasticizer [bis(2-ethylhexyl) phthalate; denoted here as PR] with a density $\rho_p = 0.985$ g/cc was used to lower the melt-viscosity of the composite.

Specimen Fabrication

The MWCNTs were first dispersed into the plasticizer using probe sonication to obtain a uniform pigment which was subsequently mixed with plastisol to produce the final composite. Following ASTM D5225, a series of viscosity tests was carried out on mixtures with different mixing ratios of the composite's ingredients (i.e., PL, PR, and MWCNT) to determine a PR/MWCNT ratio that would result in a processable pigment blend with a viscosity in the range 3–10 Pa s. This range of viscosity values is typically used for coatings on woven geogrids.[1] The room temperature in the laboratory was kept fairly constant during the tests ($T = 23 \pm 1$ °C) to minimize its impact on the viscosity of the composite. A Brookfield viscometer with a #5 spindle at a rotational speed of 5 rpm was used for the viscosity tests. MWCNT concentration was kept constant at 0.5 wt % in all tests while the PR/MWCNT ratio increased from 10 to 30. Eventually, a PR/MWCNT ratio of 24 was found to result in composites with the target viscosity.

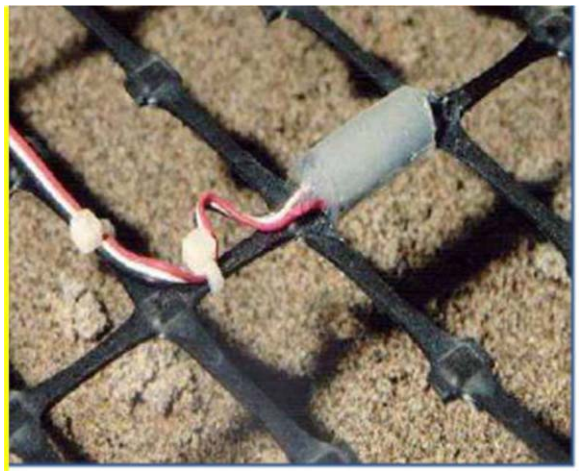

Figure 2. A strain gauge attached to a geogrid rib and covered with a protective assembly.[12] [Color figure can be viewed in the online issue, which is available at wileyonlinelibrary.com.]

To prepare the composite with the target viscosity, 2.4 g MWCNT was first manually mixed with 57.6 g of auxiliary plasticizer (PR/MWCNT = 24) to make 60 g of visually uniform pigment blend. Then, the pigment was subjected to probe sonication at 55 W for 120 min at the 50% pulse mode (i.e., 60 min net duration) to produce a pigment blend. As stated earlier, the mixing method (i.e., probe sonication) and its factors (i.e., power and duration) were selected after a comprehensive study on the effectiveness of different mixing techniques, including probe sonication, bath sonication, mechanical stirring, and batch mixing, to form a well-dispersed PVC/MWCNT composite.[21] Once the mixing of the coating composite was complete, the blended material was compression molded under 1 MPa pressure at 180 °C for 15 min, yielding 0.8 mm-thick specimens that would be used for conductivity, tensile strength, strain sensitivity, and microscopy tests. The pressure was sustained while the specimens were allowed to cool down gradually to the room temperature (typically, 23 °C) at an average rate of 2.5 °C/min. The thickness of 0.8 mm was chosen as a representative value for the coating thickness in PVC-coated polyester yarn geogrids. However, the authors' communications with geogrid manufacturers indicated that the coating thickness is not typically uniform and it is difficult to determine accurately. Nevertheless, the selected thickness is within the practical range and is not believed to influence the findings and practical implications of the study.

Conductivity Tests

Conductivity tests were carried out on nine-cm-diameter, disk-shaped MWCNT-filled PVC coating specimens at different

Table I. Properties of the MWCNT Used in this Study (as Measured, or Provided by the Supplier)

Outer diameter (nm)	Length (μm)	Aspect ratio	Carbon purity (%)	D/G ratio from Raman[a]	BET surface area[b] (m^2/g)	Density, ρ_f (g/cm^3)
7.8	0.74	95	>98	1.52	250	2.045

[a] Ratio of the G-band (graphitic carbon) to the D-band (disordered carbon) in Raman spectroscopy used as a measure for the purity and defects of CNTs. It is inversely proportional to the quality of CNTs.
[b] Nitrogen adsorption surface area measured using the BET theory (ASTM D6556; micropores included).

MWCNT concentrations to determine their percolation behavior. Three nominally identical specimens were tested for each MWCNT concentration to improve the reliability of the conductivity test results. Prior to conductivity measurements, the surface of each specimen was carefully cleaned with ethanol to ensure that it was clean and free of any residues. The specimen thickness, which was needed to calculate resistivity, was measured with a precision of 0.01 mm at four locations (i.e., at the center and three points 120° apart on the specimens circumference), and the mean value was reported as the thickness. The volume conductivity of the specimens were measured using a DC high-resistance meter (Agilent Model 4339B) in accordance with ASTM D4496. The voltage applied on the specimens was kept limited to 10 V to protect them from overheating. Also, an electrification time of 60 s was used in all measurements so as to establish a steady-state current through the specimens.

Characterization of the Composite Mechanical Properties

Factors such as the type, concentration, mechanical properties, specific surface area and aspect ratio of CNTs influence the mechanical properties of the composites in which they are embedded. Since the stress from a matrix to a CNT can only be transferred through the interface (which is the outermost layer of the CNT), only a fraction of the MWCNTs collective surface area effectively contributes to the reinforcement of the host matrix. For instance, it can be geometrically shown that the effective surface area of the MWCNT used in this study [with an outer diameter of 7.8 nm, an assumed inner diameter of 4 nm and a layer distance of 0.34 nm (7 concentric tubules)] is only 9.5% of the total surface area. A full exploitation of this effective surface area requires a perfect MWCNT dispersion to maximize the MWCNT/matrix interface.

Perfect dispersion, however, is not favorable from the electrical conductivity standpoint. Using a combination of an analytical approach and numerical and laboratory experiments, Kyrylyuk *et al.*[23] showed that for a system comprising of ingredients with different sizes and shapes (in this case, individual CNTs and bundles of different dimensions), the interplay among the ingredients could strongly influence the formation of a spanning conductive network (i.e., percolation threshold). Depending on the ease of charge transport across ingredients, this interplay could be synergetic or antagonistic. For a system containing only one conductive ingredient (as it is the case in this study), these interactions are more likely synergic and lead to a lower percolation threshold. This phenomenon was also observed by the authors in an earlier study[21] where, at a reference MWCNT concentration, the specimens of the highest electrical conductivity failed at lower stresses and strains as compared to lower-conductivity specimens. This observation implies the competing functions of CNT bundles in promoting the formation of a conductive network, while creating stress concentration zones in the composite. Interested reader is referred to a review by Grady[24] for further details.

The above discussion indicates the necessity for devising an efficient method to meet the competing mechanical and electrical requirements for a desired degree of dispersion. The probe sonication technique described earlier, however, does not address the mechanical and electrical property requirements alike. Since the coating composite is not a reinforcing element in SEGG products, more weight was given to conductivity requirements, and the potentially detrimental effect of bundling on strength was partly overlooked.

Tensile strength tests were carried out in accordance with ASTM D1708 to determine the influence of CNT concentration on the elasticity, ductility, tensile strength, and Poisson's ratio of the coating composite. Studying the Poisson's ratio of the composite was particularly useful in the analysis of its strain sensitivity, which is discussed in the subsequent sections. PVC plastisol specimens as well as specimens made of the pristine (i.e., no CNT) host matrix comprising of 75% PL and 25% PR were also tested and compared with those filled with the MWCNT. Three different strain rates were examined. A reference strain rate of 0.15%/min was used to represent the rates that could be expected in practice and practically achieved in the laboratory.[25] The tests were also carried out at faster strain rates of 2 and 10%/min to investigate the influence of loading rate on the mechanical properties of the coating composite. It is worth mentioning that the rate of strain applied on a geosynthetic structure depends on the loading type and could vary by a few orders of magnitude. Loading rates as slow as 0.01%/min have been used in the laboratory to represent those expected during the construction stage (e.g., reinforced soil embankments and retaining walls), and rates as large as 10%/min are typically prescribed in test standards (e.g., ASTM D4595[26]) for instrumented samples. In terms of strength, some of the polymers currently used in the geosynthetics industry exhibit significant sensitivity to strain rate (e.g., PE). However, the strength of polyester (as used in woven geogrids whose coating is the subject of this study) is not significantly affected by the strain rate.[27] Results of the current study were used to ensure that the mechanical properties of the coating composite would be adequate to prevent premature cracking and discontinuity in the coating when the final products (i.e., PVC-coated polyester yarn geogrids) are

Table II. Selected Test information on the Specimens Examined in this Study

MWCNT:PR:PL concentration[a] (wt %)	Strain rates in mechanical property tests (%/min)	Strain rates in strain sensitivity tests (%/min)
0:0:100	2	-
0:25:75	2	-
0.5:12:87.5	0.15, 2, 10	0.15, 2, 10
1:24:75	2	-
1.5:36:62.5	2	-

[a] PR/MWCNT = 24.
Note: Four specimens were used in mechanical tests and three other specimens were used in strain sensitivity tests listed in the table.

handled or installed in the field. The information germane to these tests is given in Table II. For each combination of CNT concentration and strain rate listed in the table, four nominally identical, dog-bone-shaped specimens were punched out from the compression-molded specimens using a die-expulsion press and tested in a tensile testing machine.

In addition to macroscopic tensile tests, an imaging technique recently developed by the authors[22] was used to investigate the subsurface effects of tensile loading on composite materials in situ and also to explore the mechanics of failure in real time. Previous studies have evaluated the failure mechanism of CNT composites based on the surface topology of previously tensioned specimens via SEM (e.g., ref. 28). SEM, however, is limited to observations near the surface of a specimen. The technique adopted in this study, in contrast, uses laser scanning confocal microscopy (LSCM) and offers a deeper and more direct insight into the dispersion characteristics of CNT bundles and the failure mechanics of CNT composites. To observe the failure mechanics of the MWCNT-filled PVC specimens subjected to tensile loading, 11-mm-long, dogbone-shaped test specimens were loaded onto a tensioning microscope stage (Micro-Vice Holder, ST Japan-USA, LLC) and subjected to a tensile strain in 2-mm (18% strain) increments by manually adjusting the lead screws of the tensioning stage. Note that no precise control could be made over the deformation rate. The specimens were imaged from the surface to a depth of 200 μm at the same position at each load increment until failure. When tears within the material were observed, they were imaged in three dimensions by acquiring a series of optical sections in the vertical direction. Interested reader is referred to the authors' earlier studies[21,29] for additional information regarding the microstructure of the composites characterized using SEM, TEM and LSCM imaging.

Tensile-Conductivity Tests

The change in the electrical resistance of a subset of the macroscopic coating specimens tested for their mechanical properties (i.e., those doped at the critical MWCNT concentration) was recorded at 0.5%-strain intervals to determine the change in their electrical conductivity as a function of the applied tensile strain. The same three strain rates that had been used in the tensile tests were used to investigate the strain rate-dependency of the coating composites tensoresistivity response. The electrical resistance of the specimens was measured using an analog Keithley electrometer and the two-point probe method in which two alligator clips 25 mm apart were attached to the specimens. Silver paint was used to enhance the electrical contact at the alligator clips attachments. Although the two-point measurement scheme includes the resistance of lead wires and contacts, this added resistance is deemed to be negligible relative to the resistance of the specimens throughout the tests. The global strain in the gauge length was measured using a digital imagery approach.[1] These strains were compared with those measured from crosshead movements to ensure that the elongation rate would be fully transmitted to the specimen and would not be partially dissipated as a result of the slippage between the specimen and the clamps of the tensile testing machine.

Real-time LSCM imaging also allowed for the measurement of the resistivity of a test specimen under tensile strain, making it possible to optically investigate the phenomenon of strain-sensitive conductivity. Specifically, samples were mounted on a manual tensioning stage [Figure 9(b)], and then imaged with a Leica SP8 LSCM using a 10×/0.3NA dry objective and a 405nm laser to excite the polymer autofluroescence. To measure the specimen's electrical conductivity under LSCM, the specimen was electrically isolated from the tensioning stage using several sheets of polyethylene, and the electrical leads were then connected directly to the specimen. The imaging of the sample and the simultaneous recording of its conductivity were carried out at the end of every 8%-strain increment in the specimen. The resulting 3D image stacks were then aligned using a rigid body registration algorithm in ImageJ (v1.50b).

RESULTS AND DISCUSSION

Electrical Conductivity

The influence of the MWCNT concentration on the volume conductivity of the PVC composite is shown in Figure 3. A

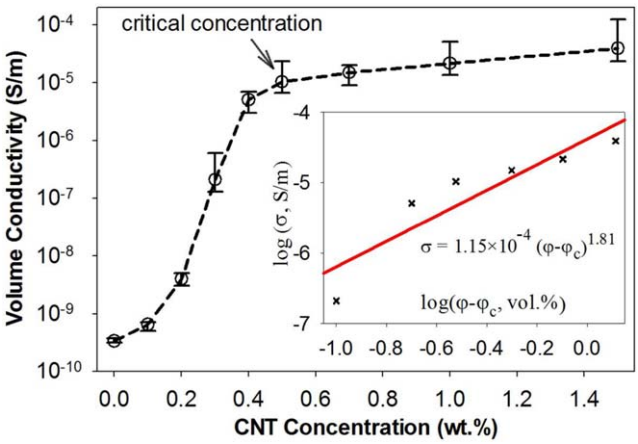

Figure 3. Volume conductivity of PVC/plastisol as a function of CNT concentration. The inset shows eq. (2) fitted to the mean value of the conductivity data. [Color figure can be viewed in the online issue, which is available at wileyonlinelibrary.com.]

Table III. Summary of the Percolation Threshold of Some Common Amorphous Polymers Filled with MWCNT

Matrix	Aspect ratio	Dispersion	φ_c (wt %)	t	Maximum conductivity (S/m)
Low viscous polyamide 12[32]	~200	Melt mixed in a conical twin-screw extruder	0.50	-	10^{-2} @ 5 wt %
High viscous polyamide 12[32]	~200	Melt mixed in a conical twin-screw extruder	2.00	-	10^{-1} @ 5 wt %
Polyimide[33]	~300	Stirred under ultrasoniocation	7.00	1.14	10^{-4} @ 12 wt %
Polymethylmethacrylate[34]	~160	Melt mixed	0.80	1.8	10^{-1} @ 8 wt %
Polystyrene[35]	~160	Ultrasoniocated	0.045	2.11	10^{-1} @ 1 wt %
Polysulfone[36]	~290	Bath sonicated	0.10	-	10^{-1} @ 1 wt %

conductivity of 3.4×10^{-9} S/m was measured for pure plastisol specimens (i.e., CNT % = 0). In the figure, the best-fitting curve, which was obtained using a least squares method, identifies a percolation threshold between 0.1–0.2 wt % in the form of an upsurge in the measured electrical conductivity with an increase in the MWCNT concentration. According to Figure 3, as the level of doping exceeds the percolation threshold, the composite enters into a region, known as the percolation region, across which a conductive network of CNTs is developed and a transition in the nature of charge transport from tunneling to partial metallic diffusive transport is observed (i.e., 0.2 wt % $< \varphi <$ 0.4 wt %). Due to the evolution of the existing or the formation of new conductive paths, the conductivity of the composite beyond the percolation region slightly increases with adding more CNTs until it levels off to 10^{-4} S/m. This level of conductivity opens the door for the composite for electrostatic discharge ($<10^{-4}$ S/m[30]) and electrostatic coating ($>10^{-5}$ S/m[31]) applications.

For comparison, the percolation threshold and conductivity of some amorphous polymers filled with MWCNT is shown in Table III. From Figure 3, the critical concentration of the fillers was estimated to be 0.5 wt % where a drastic strain-induced change in the electrical conductivity of the composite would be expected under tensile loading. Therefore, the specimens prepared for the strain sensitivity tests were doped at this concentration. It is worth noting that the tensoresistivity response of the CNT-filled composite is primarily due to increased gaps among the CNT aggregates with some minor contribution (e.g., on the order of 5%) from the tensoresistivity of the CNTs themselves.[37]

The electrical conductivity, σ, of a filled composite above the percolation threshold, φ_c, follows the scaling law (also known as the power law) proposed by Kirkpatrick[38] as:

$$\sigma = \sigma_0(\varphi - \varphi_c)^t \quad (2)$$

where σ_0 is the conductivity of the composite when it plateaus to a value close to the conductivity of the composite at high filler concentrations, φ is the volume fraction of the dispersed phase, and t is a critical exponent theoretically close to 2.0 for a three-dimensional composite filled with a randomly dispersed phase.[39] Fitting the conductivity data to the form of eq. (2) (see the inset of Figure 3) gives a critical exponent of $t = 1.81$, which is similar to that predicted by the percolation theory. The departure of the critical exponent from 2.0 could be due to the inherent drive of CNTs to bundle, which is at odds with a basic assumption in the percolation theory that the occupation of a lattice site by filler particles is essentially a random process such that the probability of a site being occupied is independent of whether or not any of its nearest neighbors is already taken.[40]

It should be noted that the strain-sensitive conductivity of filled composites can be tailored for a desired application by controlling the CNT loading, the degree of CNT dispersion and the fabrication process employed.[30,41] For instance, the composites doped at filler concentrations greater than the critical concentration possess a greater number of CNT-CNT contacts at a particular level of strain, therefore exhibiting lower strain sensitivities in tension.[42]

Mechanical Properties

The initiation and propagation of tensile fractures in the composite in real time are demonstrated in Supporting Information Video S1. It can be inferred that the growth of fracture in the specimen is governed by the comparative resistances to cracking of the polymer matrix and the inclusions (i.e., CNT bundles/individuals). Fractures were initiated from inside the largest bundles between 18–36% strain, which is close to the range of strain at failure reported for CNTs and graphene at room temperature (i.e., 8–20%[43–45]). The initiation of the fractures from bundles is possibly due to the weak van der Waals interactions between MWCNT individuals,[46] and the small shear strength between the MWCNT concentric layers (the average shear strength for high-quality graphite is approximately 0.48 MPa[47]). Inside a bundle, the stress at the tip of a crack may exceed the van der Waals forces that hold the MWCNTs together, leading to progressive cracking across the bundles. As the tensile load increased, smaller bundles within the specimen progressively ruptured perpendicular to the direction of tension while the larger bundles continued to fail through further fractal-like fracturing. As the sample approached failure, a large tear would predominate at the site of one of the largest aggregates, and propagate even under sustained constant strain. Figure 4 shows the tear across the CNT bundle at an advanced stage where the

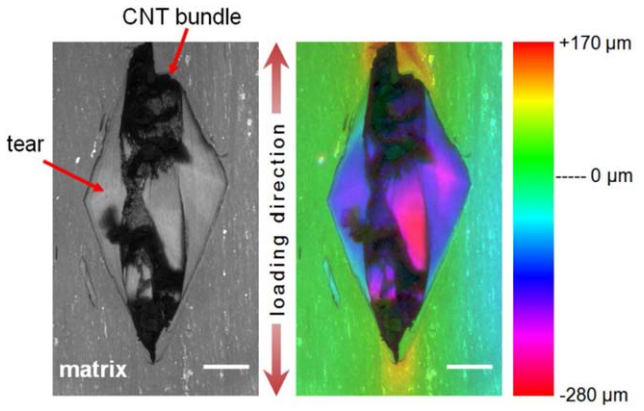

Figure 4. A grayscale maximum intensity projection (left) and corresponding 3D colorimetric surface profile (right) of a large tear forming in a composite specimen under tensile load, with a fractured CNT bundle clearly visible at the base of the tear. The 0 μm baseline on the sidebar scale refers to the elevation at the surface of the specimen at zero strain. Positive and negative values in the color bar indicate, respectively, upward and downward elevations with respect to the surface. Scale bar = 200 μm. [Color figure can be viewed in the online issue, which is available at wileyonlinelibrary.com.]

rupture has spread to the CNT-PVC interface. The initiation of the tear within the CNT bundles and its subsequent propagation to the polymer-PVC interface can be observed in Supporting Information Video S1 which accompanies this article and also in Figure 4(a) and Supplementary Movie 1 in authors' earlier study.[22] Specifically, samples were tensioned in increments of 8% strain, and then imaged down to 200 μm below the surface while the corresponding conductivity was measured. The resulting plot and corresponding image series are shown in Supporting Information Video S1.

A three-dimensional image of a large tear that formed preceding the failure of the material was acquired to better understand their formation mechanism (Figure 4). Large, fractured bundles can be observed at the base of these tears. The polymer near the tear was raised relative to the rest of the specimen, possibly causing stress relief as the material began to fail, preventing further polymer tearing around nearby aggregates. This data collectively gives a potential model of how CNT bundles in composites contribute to the failure.

Results of the conductivity tests under LSCM showed that the electrical resistance of the specimen linearly increased as strain was applied. This result can be in part attributed to the observed changes in the spatial distribution of CNT bundles and the progressive rupture of the CNT bundles as strain increased, resulting in a sequential loss of conductive pathways. This strain-sensitive conductivity of the composite is further discussed in the subsequent sections.

A typical stress-strain diagram of the composite filled with 0.5 wt % MWCNT is shown in Figure 5 which indicates an initial linear portion (demarcated by a proportional limit) followed by a strain hardening behavior. The yield point is assumed to approximately coincide with the proportional limit. The strain corresponding to the proportional limit (i.e., yield strain) was consistently observed in the tensile tests to be 36.5 ± 1%, which is close to the range of strains corresponding to the initiation of fractures inside the largest CNT bundles as observed under the microscope (i.e., 18–36%). In contrast, the "no-CNT" specimens made from 75% PL and 25% PR yielded at a strain of 18 ± 1%. This observation (i.e., advantageous effect of CNT in extending the proportional limit of polymers) is in agreement with the findings of previous studies.[48]

The strain-hardening behavior observed in Figure 5 can be ascribed to the strain-induced alignment of polymer chains.[49] The stress-strain response of the composite shows that stretching the specimens to greater extents increased the stress nonlinearly until failure occurred. Localized necking was consistently observed as the macroscopic mode of failure of the specimens.

The influence of the plasticizer and the MWCNT concentration on the mechanical properties of the composite is shown in Figure 6. It is evident from Figure 6(a) that replacing 25% of the PVC plastisol (PL) with the plasticizer (PR) significantly decreases the mean value of the tensile strength from 16.4 to 6.2 MPa (i.e., 62% reduction) while predictably allowing the composite to endure approximately 50% larger elongations before break. According to Figure 6(a), the plasticizer only slightly decreased the elastic (Young's) modulus of the PVC plastisol but significantly reduced its Poisson's ratio. These observations are due to the reducing effect of the plasticizer on the physical intramolecular forces between the polymer chains, which in turn promotes the chain mobility and thereby reduces the tensile strength and increases the ductility and compressibility of the polymer.[50]

With respect to the influence of the MWCNT on the mechanical properties of the PVC composite, Figure 6(a) shows that a composite with 0.5 wt % MWCNT has a lower ultimate strength and failure strain as compared to an otherwise identical pristine (i.e., no-CNT) composite. Figure 6(b), in contrast, indicates a fivefold increase in the tensile modulus and 59% increase in Poisson's ratio of the composite at 0.5 wt % MWCNT as compared to those of the pristine samples. This contradictory dual

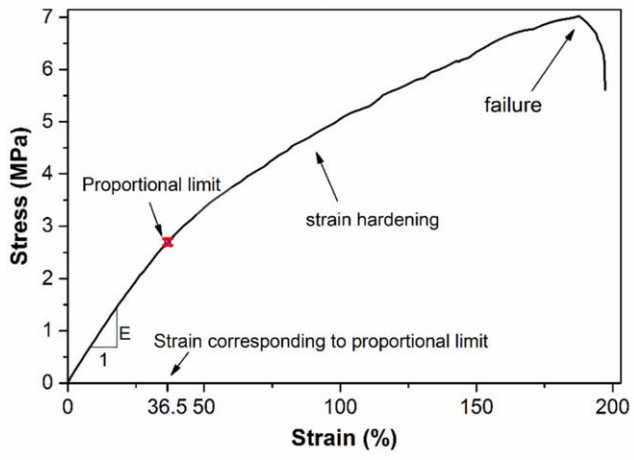

Figure 5. Stress-strain behavior of the composite filled with 0.5 wt % MWCNT. [Color figure can be viewed in the online issue, which is available at wileyonlinelibrary.com.]

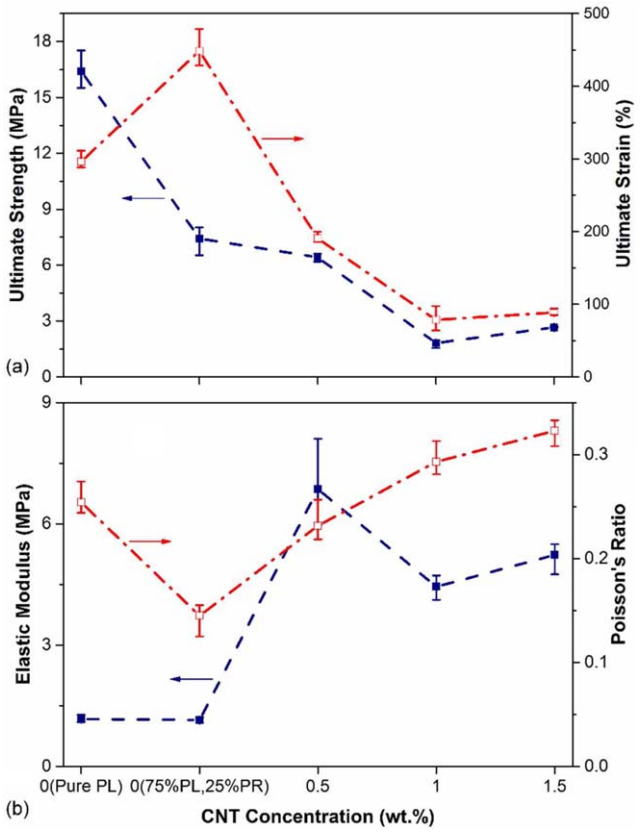

Figure 6. Influence of plasticizer and the CNT concentration on (a) the tensile strength and ultimate strain and (b) the elastic modulus and Poisson's ratio of the PVC composite (four samples were tested at each concentration shown). [Color figure can be viewed in the online issue, which is available at wileyonlinelibrary.com.]

function of MWCNTs in enhancing the tensile modulus of the composite while deteriorating its tensile strength has been reported in previous studies.[51–53] The increase in the tensile modulus and yield strain of the composite could be due to the bridging function of MWCNTs between polymer chains which forms weak physical crosslinked networks that in turn reduce the failure strain of the composite.[51]

According to Figure 6(a), increasing the MWCNT concentration to 1 wt % decreases the ultimate strength of the composite by 75% and its ultimate strain by 60% as compared to the values

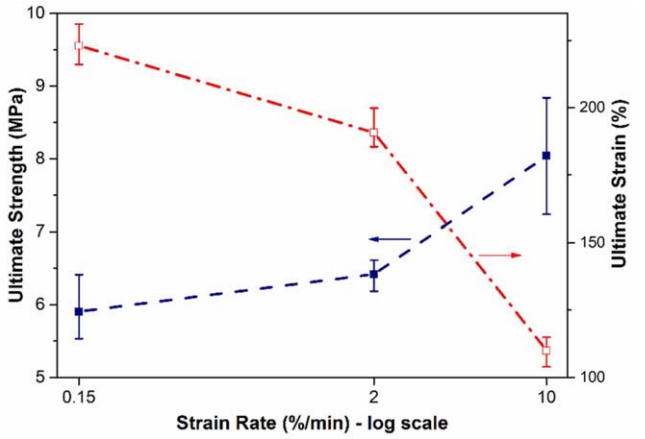

Figure 7. Influence of loading rate on the ultimate strength and strain of the composite (MWCNT = 0.5 wt %). [Color figure can be viewed in the online issue, which is available at wileyonlinelibrary.com.]

for the PL-PR matrix. It also results in 35% reduction in the elastic modulus and a 26% increase in the Poisson's ratio as compared to the 0.5%-MWCNT specimens [Figure 6(b)]. The reduction in the mechanical properties of the composite at higher filler concentrations can be attributed to the CNT aggregation at higher loading levels which in turn results in the formation of stress concentration zones at the polymer-CNT interface leading to the premature failure of the composite.[54,55] Increasing the MWCNT concentration to 1.5 wt % only slightly changed the tensile modulus and ultimate strength and strain of the composite while its Poisson's ratio continued to increase. These observations can be explained by the fact that at this level of CNT concentration (essentially one order of magnitude greater than the percolation threshold) the CNT aggregates trap the polymer molecules in the interspace between themselves and cause the composite to behave as if it was mostly made from CNTs and had a lower polymer concentration.[54] For comparison, the mechanical properties of selected amorphous and semicrystalline polymers filled with MWCNTs are summarized in Table IV.

It is worth noting that the effectiveness of the CNT reinforcement in CNT-filled polymer composites could be enhanced by improving the stress transfer at the polymer-CNT interface. The extent of the stress transfer is governed by the interfacial

Table IV. Change in Mechanical Properties of Selected Common Polymers Filled with MWCNT

Matrix	Aspect ratio	Dispersion	Concentration (wt %)	Increase in composite tensile strength (%)	Increase in composite elastic modulus (%)
PVC[56]	NR[a]	Solution mixing	0.20	84	40
Epoxy[57]	33–1 000	Solution mixing	0.50	62	54
Polyimide 12[58]	NR	Melt extrusion fiber spinning	10.00	110	110
Polystyrene[59]	446–1 167	Sonication	1.00	25 25	36 42

[a] Not reported.

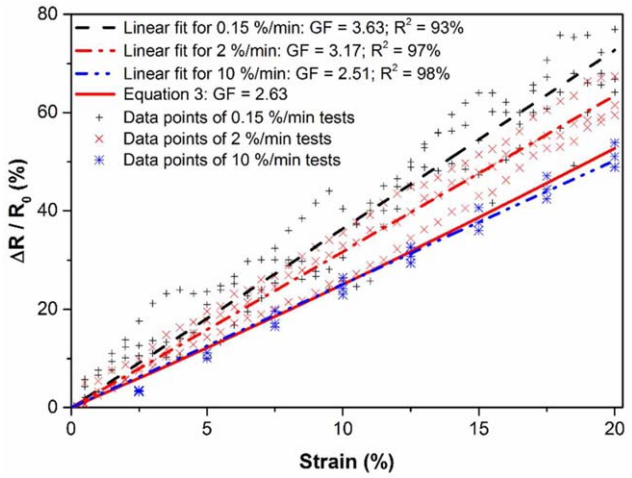

Figure 8. Strain-sensitivity response of the coating composite at the strain rates: (a) 0.15%/min, (b) 2%/min, and (c) 10%/min. Note: Data shown are for three specimens per strain rate. [Color figure can be viewed in the online issue, which is available at wileyonlinelibrary.com.]

adhesion between the CNT aggregates/particles and the polymer,[60] which is a function of the local polymer morphology at the polymer-CNT interface, and is maximized when the interfacial polymer forms a crystalline shell around CNTs.[61,62] When the interfacial polymer remains amorphous, the weak van der Waals interactions at the polymer-CNT interface impede the complete stress transfer, hindering the full exploitation of the reinforcing function of CNTs.[63,64] Ensuring an effective stress transfer in MWCNTs with greater surface areas is even more challenging due to the difficulties associated with impregnating and dispersing mesoporous MWCNTs.[52]

Figure 7 shows ultimate strength and failure (ultimate) strain values of MWCNT-filled composites as a function of strain rate at room temperature. Results show higher ultimate strength and lower failure strains for the specimens when tested at higher strain rates, which indicates a viscoelastic behavior. Strain-rate dependency is a common trait in the mechanical response of polymeric materials and could be explained by a reduction in the molecular mobility of the polymer at higher strain rates resulting in a more brittle behavior for the composite.[49,65]

Tensoresistivity Response of the Coating Composite

Figure 8 shows the strain sensitivity of the coating specimens' electrical resistance (tensoresistivity) at different strain rates in normalized form ($\Delta R/R_0$) as a function of the applied tensile strain. The real-time changes in the resistivity of a test specimen under tensile strain in LSCM is also shown in Figure 9 and Supporting Information Video S1. The test results are approximated with linear regression lines on the basis of eq. (1) resulting in gauge factors equal to 3.63, 3.17, and 2.51 for the strain rates 0.15, 2, and 10%/min, respectively, for the large-scale specimens (Figure 8), and a gauge factor of 2.09 for the specimen tested in LSCM (Figure 9). The increase in resistivity could be in part attributed to the observed changes in the spatial distribution of CNT bundles and the progressive rupture of the CNT bundles as strain increased (Supporting Information Video S1), resulting in a sequential loss of conductive pathways.

Although the gauge factors are comparable to those obtained for CB-filled PVC composites,[1,9] the composite studied here exhibited a considerably lower scatter in its strain sensitivity response, which is attributed to the fibrous geometry of CNTs as opposed to the agglomerated and generally bulkier structure of CBs. The GF values obtained are within the range of those for metal strain gauges (0.74–5.1[4]). For comparison, the GF values of some polymer composites filled with CB or MWCNT are summarized in Table V. The significant GF values obtained for the MWCNT-filled PVC composites that were fabricated and tested in this study together with consistently high R^2 values for a wide range of strains (i.e., 20% in tensile testing and 80% in LSCM experiments) provide promising evidence for their strong potential in strain sensing and damage detection applications.[17]

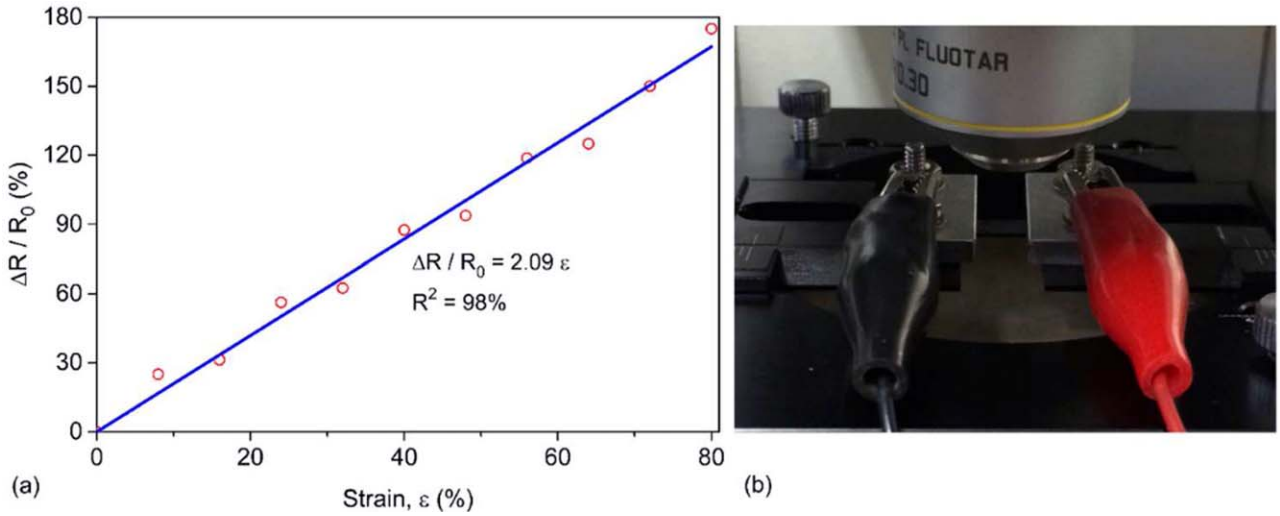

Figure 9. (a) Strain sensitivity of a sample conductivity during imaging and (b) the experimental setup, with a test sample loaded onto the tensioning stage. [Color figure can be viewed in the online issue, which is available at wileyonlinelibrary.com.]

Table V. Gauge Factors Reported for Selected Filled Polymer Composites

Matrix	Filler	Aspect ratio	Dispersion	Concentr. (wt %)	GF
PVC plastisol[a]	CB	NA[a]	Mechanical stirrer	1.50	3.2–4.6
Epoxy vinyl ester[66]	MWCNT	63–307	Mechanical stirrer and sonicator	0.30	2.6
Polycarbonate[67]	MWCNT	NR[b]	Injection molder	5.00	3.65–6.2
Bisphenol-F epoxy[68]	MWCNT	100	Planetary mixer	1.00	23
Polyethylene oxide[4]	MWCNT	50–500	Magnetic stirrer and sonicator	0.90–2.50	3.7
Poly(methyl methacrylate)[69]	MWCNT	50–8 300	Mechanical stirrer and sonicator	1.00	15

[a] Not applicable.
[b] Not reported.

Greater tensoresistivity of the coating composite at slower loading rates as observed in Figure 8 suggests that stress relaxation (which is greater at slower rates) is more able to disrupt CNT-CNT interactions vs. a more affine deformation corresponding to a faster rate. This is also evident from the lower gauge factor of 2.09 obtained in the real-time microscopic tests (see Supporting Information Video S1), where deformation was applied incrementally and at a fast rate.

It is worth mentioning that the piezoresistive/tensoresistive response (gauge factor) of a material is made of an intrinsic component, $\Delta\rho/\varepsilon\rho$, caused by an increase in the tunneling resistances, and a geometric component, $1 + 2\nu$, where ν is the Poisson's ratio of the material.[70] For the composite filled with 0.5 wt % MWCNT, since the mean value of ν is 0.23 [Figure 6(b)], the contribution of the geometrical effect to its GF value is 1.46. Therefore, the predominant component of the composite tensoresistivity response shifts from the intrinsic component for the specimens tested at slower rates to the geometric component for those tested at faster rates.

The tensoresistivity of MWCNT composites can be predicted using the method proposed by Park *et al.*[4] The method predicts the electrical conductivity of a specimen, σ_s, subjected to a uniaxial strain of ε_x as:

$$\sigma_s = \sigma_0\left(\frac{\varphi}{e+1} - (e+1)\varphi_c\right)^t \quad (3)$$

where σ_0, φ, and φ_c are the same as those defined in eq. (2) and e is the volumetric strain of the specimen defined as:

$$e = (1+\varepsilon_x)(1-\nu_{xy}\varepsilon_x)(1-\nu_{xz}\varepsilon_x) - 1 \quad (4)$$

where ν_{xy} and ν_{xz} are the Poisson's ratios determined from the ratio of the strains in the transverse directions (y and z directions), respectively, to the strain in the axial direction (x direction) due to axial loading in x direction. Assuming the composite is isotropic, ν_{xy} and ν_{xz} are the same and equal to 0.23 [Figure 6(b)]. Substituting the required values into eqs. (3) and (4) yields a GF value of 2.63 (the solid line in Figure 8), which is well within the GF values obtained in experiments.

CONCLUSIONS

Mechanical properties and tensoresistivity of a PVC/MWCNT composite subjected to tensile loading were studied at different strain rates to examine their potential use in sensor-enabled geogrids. In addition to large-scale tests in a tensile testing machine, one specimen was stretched under a laser scanning confocal microscope and its conductivity was simultaneously measured to understand the failure mechanism of the composite and the microstructural changes contributing to its strain-sensitive conductivity response. The large-scale mechanical response of the composite was found to be linear at low strains leading to a strain hardening behavior at larger strains. It was found that on average, composite samples with 0.5 wt % MWCNT concentration resulted in a 57% reduction in the ultimate (failure) strain and a fivefold increase in their tensile modulus when compared to otherwise identical pristine PVC-plasticizer samples. The failure mechanism of the composite was observed to be initiated from inside the largest CNT bundles, followed by smaller bundles and debonding at CNT/polymer interfaces. The gauge factors for the tensoresistivity response of the composite samples were found to have a fairly low scatter and comparable to those of commercially available strain gauges over a large range of strains which is practically significant (i.e., $\varepsilon \leq 20\%$). Therefore, MWCNT-filled PVC coatings for geogrids hold promise as a viable solution for performance monitoring and damage detection in a variety of geotechnical, transportation and environmental engineering applications, especially those involving geosynthetics. The strain-sensitive coating composite developed in this study facilitates measuring strains at a significant number of locations in geosynthetic products (e.g., geogrids), which will help improve the accuracy and reliability of the performance data at anticipated lower costs as compared to existing solutions.

ACKNOWLEDGMENTS

Plastisol was donated by MarChem Southeast Corporation and CNTs (product ID: SWeNT® SMW-100) were provided by Dr. Brian Grady of the University of Oklahoma.

REFERENCES

1. Hatami, K.; Hassanikhah, A.; Yazdani, H.; Grady, B. *J. Nanomech. Micromech.* **2014**, *4*, A4013016.
2. Chung, D. D. L. *Carbon* **2012**, *50*, 3342.
3. Srivastava, S.; Tchoudakov, R.; Narkis, M. *Polym. Eng. Sci.* **2000**, *40*, 1522.
4. Park, M.; Kim, H.; Youngblood, J. P. *Nanotechnology* **2008**, *19*, 055705.

5. Service, R. F. *Science* **2003**, *301*, 909.
6. Bashir, T.; Ali, M.; Persson, N. K.; Ramamoorthy, S. K.; Skrifvars, M. *Textile Res. J.* **2014**, *84*, 323.
7. Kang, T. J.; Choi, A.; Kim, D. H.; Jin, K.; Seo, D. K.; Jeong, D. H.; Hong, S. H.; Park, Y. W.; Kim, Y. H. *Smart Mater. Struct.* **2011**, *20*, 015004.
8. Chung, D. D. L. *Adv. Cement Res.* **2004**, *16*, 167.
9. Yazdani, H.; Hatami, K.; Khosravi, E.; Harper, K.; Grady, B. P. *Carbon* **2014**, *79*, 393.
10. Watts, G. R. A.; Brady, K. C.; Greene, M. J. The Creep of Geosynthetics; Thomas Telford: London, UK, **1998**.
11. Warren, K. A.; Christopher, B.; Howard, I. L. *Geosynt. Int.* **2010**, *17*, 403.
12. Hatami, K.; Grady, B. P.; Ulmer, M. C. *J. Geotech. Geoenviron. Eng.* **2009**, *135*, 863.
13. Hatami, K.; Grady, B.; Ulmer, M. *J. Geotech. Geoenviron. Eng.* **2011**, *137*, 435.
14. Fathi, A.; Hatami, K.; Grady, B. P. *Polym. Eng. Sci.* **2012**, *52*, 549.
15. Yazdani, H.; Hatami, K.; Hawa, T.; Grady, B. P. GeoCongress **2013**: Stability and Performance of Slopes and Embankments III, 2013/02/25/2013, p 1522.
16. Koerner, R. M. Designing with Geosynthetics, 6th ed.; Xlibris, Corp., **2012**; Vol. *1*.
17. Yazdani, H.; Hatami, K.; Grady, B. P. *J. Test. Evaluation* **2016**, *44*, 20140501.
18. Broza, G.; Piszczek, K.; Schulte, K.; Sterzynski, T. *Comp. Sci. Technol.* **2007**, *67*, 890.
19. Mamunya, Y.; Boudenne, A.; Lebovka, N.; Ibos, L.; Candau, Y.; Lisunova, M. *Comp. Sci. Technol.* **2008**, *68*, 1981.
20. Mamunya, Y. P.; Levchenko, V. V.; Rybak, A.; Boiteux, G.; Lebedev, E. V.; Ulanski, J.; Seytre, G. *J. Non Cryst. Solids* **2010**, *356*, 635.
21. Yazdani, H.; Smith, B. E.; Hatami, K. *Comp. Part A: Appl. Sci. Manuf.* **2016**, *82*, 65.
22. Smith, B.; Yazdani, H.; Hatami, K. *Comp. Part A: Appl. Sci. Manuf.* **2015**, *79*, 23.
23. Kyrylyuk, A. V.; Hermant, M. C.; Schilling, T.; Klumperman, B.; Koning, C. E.; van der Schoot, P. *Nat. Nanotechnol.* **2011**, *6*, 364.
24. Grady, B. P. *Macromol. Rapid Commun.* **2010**, *31*, 247.
25. Hatami, K.; Bathurst, R. *J. Can. Geotech. J.* **2005**, *42*, 1066.
26. Astm, D. In Annual Book of ASTM Standards; ASTM International: West Conshohocken, PA, **2011**.
27. Boyle, S. R.; Gallagher, M.; Holtz, R. D. *Geosynt. Int.* **1996**, *3*, 205.
28. Shokrieh, M. M.; Saeedi, A.; Chitsazzadeh, M. *J. Nanostruct. Chem.* **2013**, *3*, 1.
29. Yazdani, H.; Smith, B.; Hatami, K. In Carbon Nanotechnology; Milne, W. I.; Cole, M.; Mitura, S., Eds.; One Central Press: Manchester, UK, **2016**.
30. Ferreira, A.; Rocha, J. G.; Ansón-Casaos, A.; Martínez, M. T.; Vaz, F.; Lanceros-Mendez, S. *Sens. Actuators A Phys.* **2012**, *178*, 10.
31. Baughman, R. H.; Zakhidov, A. A.; Heer, W. A. D. *Science* **2002**, *297*, 787.
32. Socher, R.; Krause, B.; Hermasch, S.; Wursche, R.; Pötschke, P. *Comp. Sci. Technol.* **2011**, *71*, 1053.
33. Zhu, B. K.; Xie, S. H.; Xu, Z. K.; Xu, Y. Y. *Comp. Sci. Technol.* **2006**, *66*, 548.
34. Logakis, E.; Pandis, C.; Pissis, P.; Pionteck, J.; Pötschke, P. *Comp. Sci. Technol.* **2011**, *71*, 854.
35. Shrivastava, N. K.; Khatua, B. B. *Carbon* **2011**, *49*, 4571.
36. Bautista-Quijano, J. R.; Avilés, F.; Aguilar, J. O.; Tapia, A. *Sens. Actuators A Phys.* **2010**, *159*, 135.
37. Oliva-Avilés, A. I.; Avilés, F.; Seidel, G. D.; Sosa, V. *Comp. Part B Eng.* **2013**, *47*, 200.
38. Kirkpatrick, S. *Rev. Mod. Phys.* **1973**, *45*, 574.
39. Gingold, D. B.; Lobb, C. *J. Phys. Rev. B* **1990**, *42*, 8220.
40. Kawakatsu, T. Statistical Physics of Polymers: An Introduction; Springer-Verlag Berlin Heidelberg: Germany, **2004**.
41. Loh, K. J.; Lynch, J. P.; Shim, B. S.; Kotov, N. A. *J. Intell. Mater. Syst. Struct.* **2008**, *19*, 747.
42. Kang, I.; Schulz, M. J.; Kim, J. H.; Shanov, V.; Shi, D. *Smart Mater. Struct.* **2006**, *15*, 737.
43. Eftekhari, M.; Hatefi Ardakani, S.; Mohammadi, S. *Theor. Appl. Fracture Mech.* **2014**, *72*, 64.
44. Eftekhari, M.; Mohammadi, S.; Khoei, A. R. *Comput. Mater. Sci.* **2013**, *79*, 736.
45. Yazdani, H.; Hatami, K. *Model. Simul. Mater. Sci. Eng.* **2015**, *23*, 065004.
46. Yu, M. F.; Lourie, O.; Dyer, M. J.; Moloni, K.; Kelly, T. F.; Ruoff, R. S. *Science* **2000**, *287*, 637.
47. Soule, D. E.; Nezbeda, C. W. *J. Appl. Phys.* **1968**, *39*, 5122.
48. Tang, W.; Santare, M. H.; Advani, S. G. *Carbon* **2003**, *41*, 2779.
49. Sarva, S.; Boyce, M. *J. Mech. Mater. Struct.* **2007**, *2*, 1853.
50. Stark, T. D.; Choi, H.; Diebel, P. W. *Geosynt. Int.* **2005**, *12*, 99.
51. Xia, H.; Wang, Q.; Qiu, G. *Chem. Mater.* **2003**, *15*, 3879.
52. Breton, Y.; Désarmot, G.; Salvetat, J. P.; Delpeux, S.; Sinturel, C.; Béguin, F.; Bonnamy, S. *Carbon* **2004**, *42*, 1027.
53. Ogasawara, T.; Ishida, Y.; Ishikawa, T.; Yokota, R. *Comp. Part A: Appl. Sci. Manuf.* **2004**, *35*, 67.
54. Song, Y. S.; Youn, J. R. *Carbon* **2005**, *43*, 1378.
55. Blond, D.; Barron, V.; Ruether, M.; Ryan, K. P.; Nicolosi, V.; Blau, W. J.; Coleman, J. N. *Adv. Funct. Mater.* **2006**, *16*, 1608.
56. Shi, J. H.; Yang, B. X.; Pramoda, K. P.; Goh, S. H. *Nanotechnology* **2007**, *18*, 375704.
57. Špitalský, Z.; Matějka, L.; Šlouf, M.; Konyushenko, E. N.; Kovářová, J.; Zemek, J.; Kotek, J. *Polym. Compos.* **2009**, *30*, 1378.

58. Sandler, J. K. W.; Pegel, S.; Cadek, M.; Gojny, F.; van Es, M.; Lohmar, J.; Blau, W. J.; Schulte, K.; Windle, A. H.; Shaffer, M. S. P. *Polymer* **2004**, *45*, 2001.

59. Qian, D.; Dickey, E. C.; Andrews, R.; Rantell, T. *Appl. Phys. Lett.* **2000**, *76*, 2868.

60. Gojny, F. H.; Wichmann, M. H. G.; Fiedler, B.; Schulte, K. *Comp. Sci. Technol.* **2005**, *65*, 2300.

61. Cadek, M.; Coleman, J. N.; Barron, V.; Hedicke, K.; Blau, W. J. *Appl. Phys. Lett.* **2002**, *81*, 5123.

62. Coleman, J. N.; Cadek, M.; Blake, R.; Nicolosi, V.; Ryan, K. P.; Belton, C.; Fonseca, A.; Nagy, J. B.; Gun'ko, Y. K.; Blau, W. J. *Adv. Funct. Mater.* **2004**, *14*, 791.

63. Bhattacharyya, A. R.; Pötschke, P.; Häußler, L.; Fischer, D. *Macromol. Chem. Phys.* **2005**, *206*, 2084.

64. Lahiff, E.; Leahy, R.; Coleman, J. N.; Blau, W. J. *Carbon* **2006**, *44*, 1525.

65. Richeton, J.; Ahzi, S.; Vecchio, K. S.; Jiang, F. C.; Adharapurapu, R. R. *Int. J. Solids Struct.* **2006**, *43*, 2318.

66. Ku-Herrera, J. J.; Avilés, F. *Carbon* **2012**, *50*, 2592.

67. Parmar, K.; Mahmoodi, M.; Park, C.; Park, S. S. *Smart Mater. Struct.* **2013**, *22*, 075006.

68. Hu, N.; Karube, Y.; Arai, M.; Watanabe, T.; Yan, C.; Li, Y.; Liu, Y.; Fukunaga, H. *Carbon* **2010**, *48*, 680.

69. Pham, G. T.; Park, Y. B.; Liang, Z.; Zhang, C.; Wang, B. *Comp. Part B: Eng.* **2008**, *39*, 209.

70. Costa, P.; Silva, J.; Ansón-Casaos, A.; Martinez, M. T.; Abad, M. J.; Viana, J.; Lanceros-Mendez, S. *Comp. Part B: Eng.* **2014**, *61*, 136.